Princeton Plasma Physics Laboratory

PPPL-5211

Localization of ULF waves in multi-ion plasmas of the planetary magnetosphere

Eun-Hwa Kim, Jay R. Johnson, and Dong-Hun Lee[1]

[1] School of Space Research, Kyung Hee University, Yongin, Korea

November 2015

Prepared for the U.S. Department of Energy under Contract DE-AC02-09CH11466.

Localization of ULF waves in multi-ion plasmas of the planetary magnetosphere

Eun-Hwa Kim[†,1], Jay R. Johnson[1], and Dong-Hun Lee[2]

[†] Corresponding author: E.-H. Kim, Princeton Center for Heliophysics and Princeton Plasma Physics Laboratory, Princeton University, P.O. Box 0451, Princeton, NJ 08543-0451, USA (ehkim@pppl.gov)

[1] Princeton Center for Heliophysics and Princeton Plasma Physics Laboratory, Princeton University, Princeton, New Jersey, USA

[2] School of Space Research, Kyung Hee University, Yongin, Korea

Abstract

By adopting 2D time-dependent wave code, we investigate how mode-converted waves at the ion-ion hybrid resonance and compressional waves propagate in 2D density structures with wide range of field-aligned wavenumber to background magnetic fields. The simulation results show that the mode-converted waves have continuous band across the field line consistent with previous numerical studies. These waves also have harmonic structures in frequency and are also localized in the field-aligned heavy ion density well. Our results thus emphasis an importance of field-aligned heavy ion density structure on ULF wave propagation and suggest the ion-ion hybrid waves can be localized in different location along the field line.

Keywords

Ultra-low frequency waves

Electromagnetic ion cyclotron waves

Ion-ion hybrid resonance

Mode conversion

Wave-wave interaction

1. Introduction

Plasmas support a wide variety of plasma waves that carry information to remote observers (e.g., Lee et al., 2014; Hwang, 2015). Ultra-low frequency (ULF) waves in the ion cyclotron range of frequency, which can interact with electron and ions (e.g., Rauch and Roux, 1982; Horne and Thorne, 1997; Song et al., 1999), are often observed in the planetary magnetospheres (e.g., Russell et al., 2008; Boardsen et al., 2012) as well as Earth's magnetosphere and ionosphere (e.g., Kim et al., 2010, 2011).

In the ion cyclotron frequency range, the wave dispersion relations can be simplified to

$$n_\perp^2 \cong \frac{(\varepsilon_R - n_\parallel^2)(\varepsilon_L - n_\parallel^2)}{(\varepsilon_S - n_\parallel^2)}, \tag{1}$$

where n is the wave refractive index (kc/ω), subscripts $\perp$ and $\parallel$ represent the perpendicular and parallel directions to the ambient magnetic field ($\mathbf{B}_0$), respectively. $\varepsilon_{R,L,S}$ are the tensor elements for multiple ions,

$$\varepsilon_R(\varepsilon_L) \cong \frac{1}{\omega}\frac{\omega_{pe}^2}{\Omega_e}\left[\pm 1 - \sum_{ion}\frac{\eta_j \Omega_j}{\omega \pm \Omega_j}\right] \tag{2}$$

and

$$\varepsilon_S \cong \frac{\omega_{pe}^2}{\Omega_e}\sum_{ion}\frac{\eta_j \Omega_j}{\Omega_j^2 - \omega^2}, \tag{3}$$

where $\omega = 2\pi f$ is an angular frequency, $\omega_{pj(e)}$ and $\Omega_{j(e)}$ are plasma and cyclotron frequencies of jth ion (electron), and $\eta_{ion} = N_{ion}/N_e$ is the ratio of ion to electron density (N_e).

For perpendicular propagation ($n_\parallel \to 0$), the dispersion relation in Eq. (1) exhibits a resonance ($n_\perp \to \infty$) where $\varepsilon_S(\omega_{bb})=0$,

$$\omega_{bb}^2 = \Omega_1 \Omega_2 \frac{\eta_1 \Omega_2 + \eta_2 \Omega_1}{\eta_1 \Omega_1 + \eta_2 \Omega_2}, \tag{4}$$

which is the Buchsbaum frequency (bi-ion frequency) (Buchsbaum, 1960). For oblique propagation ($n_{\|}\neq 0$), the perpendicular resonance ($n_{\perp}\rightarrow\infty$) occurs at the location $\left(\omega_{ii}(x)=\omega\right)$ where

$$n_{\|}^{2}\left(\omega=\omega_{ii}\right)=\varepsilon_{S}\left(\omega=\omega_{ii}\right). \tag{5}$$

Between each pair of gyrofrequencies, there is a mode conversion location that is referred to as the ion-ion hybrid (IIH) resonance and the frequency (ω_{ii}) called the IIH frequency (e.g., Lee et al., 2008). When fast compressional waves (FWs), propagating across magnetic flux surfaces, satisfy the IIH resonance condition encounter inhomogeneity in the heavy ion concentration and/or magnetic field strength, it may be possible for the wave to satisfy the resonance condition (5), where energy from incoming FWs concentrates at the IIH resonance location and mode converts to field-aligned propagating IIH waves that satisfy the dispersion relation of $n^{2}_{\|}\sim\varepsilon_{S}$.

Because of the different conditions in planetary magnetospheres, the IIH resonance can exhibit significant differences. At Mercury, where the magnetic field is relatively weak, the wavelength of field-aligned modes can be comparable to the size of the magnetosphere. Therefore, IIH waves are oscillate globally along the magnetic field lines at Mercury, similar to the field line resonance at Earth (Othmer et al., 1999, Glassmeier et al., 2003; Glassmeier et al., 2004; Klimushkin et al., 2006; Kim et al., 2008, 2011, 2013, 2015a, 2015b). On the other hand, at Earth, the magnetic field strength is larger and the wavelength is shorter, which typically localizes mode converted waves between the Buchsbaum cutoff locations, which occur around 10 degrees latitude. The modes that result from mode conversion are typically linearly polarized EMIC waves can be generated via mode conversion near the ion-ion hybrid (IIH) resonance location (Lee et al., 2008). These waves have a significantly different polarization from EMIC waves that are excited by proton temperature anisotropy (e.g., Cornwall, 1965; Kennel and Petschek, 1966; Williams and Lyons, 1974a, 1974b; Taylor and Lyons, 1976). Because the incoming FW absorption at the IIH resonance (e.g., the generation of linearly polarized EMIC waves) occurs in the limited wave frequency and heavy ion density ratio, the linearly polarized waves are also suggested to as a diagnostic tool to estimate heavy ion density ratio (e.g., Kim et al., 2015c).

In planetary magnetospheres, as the mode-converted IIH waves near the magnetic equator propagate to higher magnetic latitudes, the waves reach cutoff ($n_{||} = 0$ and $\varepsilon_S = 0$) at $\omega = \omega_{bb}$ and parallel resonance ($n_{||} \rightarrow \infty$ and $\varepsilon_S \rightarrow \infty$) locations at $\omega = \Omega_{ion}$. Because the IIH waves are partially reflected at the Buchsbaum resonance location where $\omega = \omega_{bb}$, the waves are possibly localized near the magnetic equator between two Buchsbaum resonance locations (e.g., Klimushkin et al., 2010; Vincena et al., 2011). The localization of mode-converted IIH wave is referred to as “ion-ion hybrid Alfven resonator” and experimentally detected in the laboratory plasmas (Vincena et al., 2011, 2013, Farmer and Morales, 2014).

Recent 2D full wave simulations of Mercury’s dipolar magnetosphere (Kim et al., 2015a), which assumed constant particle densities, clearly showed the reflection of the IIH resonant waves at the Buchsbaum resonance location and wave tunneling through wave stopgap between cutoff and resonance. However, as shown in Eq. (4), the Buchsbaum frequency is a function of heavy ion density concentration ratio as well as the ambient magnetic field strength. Therefore, it is useful to examine the solutions of IIH resonant waves in more detail to determine how the wave structure and absorption of energy depend on variations in the magnetic field strength and density.

In this paper, we use a multi-ion fluid wave code to demonstrate mode conversion that occurs at the IIH resonance when impulsive FWs enter the plasma with 2D inhomogeneous density structure, which is assumed to be result from sputtering of material from the surface of Mercury. We fine that mode converted IIH waves can be localized in the density well along the magnetic field line, and also exhibit harmonic frequency structure.

2. Numerical Results

We employ the fluid wave simulation model, which has been developed by Kim and Lee (2003). Similar to previous wave simulations (Kim et al., 2008, 2013), we adopt the plasma conditions at Mercury, thus the background magnetic field B_0=86nT and the electron density N_e=3cm^{-3} are assumed to be constant. The ambient magnetic field lies in the z direction and the inhomogeneity is introduced in the x-z plane. We limit ourselves that all perturbations are proportional to $\exp(ik_y y)$, where k_y is the given wavenumber in the y direction, and for simplicity, k_y is assumed to be 0. Because the Mercury's magnetopause is located near 1.4 R_M (Anderson et al., 2011), we assume a shorter radial distance of 1 R_M than the magnetopause location in x direction, where R_M is Mercury's radius. The length in z direction (L_z) is assumed to L_z=0.93R_M which is similar to field line length at L_M=1.5 in dipole coordinate, where L_M is magnetic L-shell number at Mercury. We adopt a grid with dimension $N_x \times N_z$ = 300×100 and to save computing time, the ratio of proton mass (m_H) to electron mass (m_e) is assumed to be 100 (m_H/m_e=100).

Because sodium is one of the major heavy ions at Mercury (e.g., Zurbuchen et al., 2011; Raines et al., 2014), similar to previous numerical studies (Kim et al., 2008, 2011) we adopt an electron-proton-sodium plasma. We assume the sodium density (N_{Na}) has a minimum value (i.e., sodium density well) at the center of the simulation domain as shown in Figure 1. The electron density is assumed to be sum of the ion densities. Thus, the proton density ratio to the electron density is $\eta_{\mathrm{H}} = N_{\mathrm{H}}/N_{\mathrm{e}} = 1 - \eta_{\mathrm{Na}}$, where $\eta_{\mathrm{Na}} = N_{\mathrm{Na}}/N_{\mathrm{e}}$, and η_{H} has maximum in the middle of the simulation domain.

The simulation is driven by imposing an impulse in E_y at $X=x/L_x=1$ during the interval $0\leq\tau=t/t_{ci}\leq2.5$, where $t_{ci}=2\pi/\Omega_H$ as shown in Figure 2a. Figure 2b shows the initial field-aligned wave structures along $Z=z/L_z$ at $X=1$. Because the width of the source is closely related to the initial wavevector, the wide source corresponds to more perpendicular propagation. The boundaries become perfect reflectors after the impulsive stimulus ends (τ = 2.5), thus the total energy in the box model will remain constant in time after this interval.

We store the time history of the electromagnetic fields at each grid point (X, Z) during the simulation run time ($0 < \tau < 55$) and obtain the wave power spectra through the fast Fourier transform. To examine wave properties along and across the magnetic field line, we selected two points in X and Z, X_0 (Z_0) = 0.55 and 0.7, respectively, as shown in Figure 1. Under the given condition, because the density inhomogeneity lies in X and Z directions, E_x represent the mixture of the IIH resonant wave and FW modes, while E_y shows pure FW mode.

Figure 3a and 3b show the time history of the transverse component (to $\mathbf{B}_0$) of the electric fields (E_x and E_y) along X at $Z=Z_0$. In this figure, the FWs launched at $X=1$ propagate toward the Na^+ density well and reach the inner boundary at $X=0$. The evidence of a wave stopgap and wave tunneling near $X\sim0.5$ at $Z=0.55$ are also found in E_y. On the other hand, as soon as the FW packet reaches the region, $0.5<X<1$, the IIH resonant wave modes exhibit standing oscillations in E_x and the period of the oscillation decreases as X decreases (decreasing η_{Na} concentration). However, for $X<0.5$, no oscillation of the mode-converted waves is found in E_x.

The wave time history along the Z direction at $X=X_0$ is plotted in Figure 3c and 3d. In this case, the FWs in the E_y component reach the boundaries in a short time and reflect. In this figure, it can be seen that E_y in each location along Z has different period of wave oscillation. Near the boundaries, E_y exhibits a mixture of long and short period waves, while long period waves only appear near the center of Z direction. On the other hand, waves with E_x polarization are localized within the middle of Z. As shown in Figure 3a and 3b, wave periods at Z=0.55 is lower than at Z=0.7.

Figure 4 shows wave spectra of E_x and E_y. E_x in Figure 4a and b shows a strong continuous band at the IIH resonance wave in the X direction, which is consistent with previous numerical results. Because the field-aligned wavenumber is not fixed, several harmonics of the IIH waves can be seen. The wave power spectra along Z in Figure 4c and 4d also clearly show that the mode-converted IIH waves have several eigenfrequencies and they are localized between the two Buchsbaum resonance locations. The second harmonic of the IIH waves have a node near Z=0.55 and antinode near Z=0.7; therefore, E_x only shows a strong fundamental band in Figure 4a but strong fundamental and second harmonics in Figure 4b.

The FWs in E_y component propagate to the middle of the simulation domain and most energy in high frequencies, where the strong continuous band appears in E_x, cannot reach the inner boundary at X=0. The inaccessibility occurs because FWs propagating from Na^+-rich to H^+-rich plasma directly encounter the IIH resonance location where strong energy absorption occurs (up to 100% as predicted by Lee et al., (2008)). For waves with ω/Ω_H<0.3, the FWs are partially absorbed at the IIH resonance location and the rest of the energy can reach the FW cutoff locations where $n^2_{||}=\varepsilon_L$, and then encounter another IIH resonance location at X<0.5. However, when waves propagate from H^+-rich to Na^+-rich plasma, wave absorption only occurs in the limited frequencies and the absorption coefficient is much lower than the opposite case, no continuous band at the IIH resonance appeared.

3. Discussion

In this paper, we show how mode-converted IIH waves can be localized in a heavy ion density well in slab coordinates. Because the Buchsbaum frequency increases as the heavy ion density concentration ratio increases, an irregular ion density structure along the field line can lead to an asymmetric structure of the Buchsbaum frequency. Our results, therefore, emphasize the importance of field-aligned heavy ion density structures on ULF wave propagation. It should be noted that equilibria in magnetospheres with rotational disks generally have density structures along the magnetic field line due to centrifugal acceleration, which concentrates the heavy ions into the magnetodisk.

In Figure 5, we demonstrate how asymmetry the ion density ratio affects to field-aligned wave propagation. We assumed the field-aligned density structure of η_{Na} and η_{H} at Mercury as shown in Figure 5a and calculated the Buchsbaum frequency as shown in Figure 5b. When plasma contains a constant sodium density of η_{Na}=20% and the Buchsbaum frequency (ω_{bb0}), wave frequencies that are higher than highest Buchsbaum frequency do not encounter the cutoff condition, thus can globally oscillate, which is similar to the field-line resonance at Earth (e.g., Lee and Lysak, 1989). However, for asymmetric structure of the ion density, waves generated near the magnetic equator with 1Hz can be localized between $-21.7<\Lambda<15$. In addition, if the waves can tunnel through the small bump of the Buchsbaum frequency, the waves can reach the secondary density well and are possibly localized between $20.5<\Lambda<27.9$.

Interestingly, the Buchsbaum resonance is also a cutoff condition of the LHP EMIC waves (Johnson et al., 2005). At Earth's magnetosphere, as these waves propagate along $\mathbf{B}_{0,}$ wave normal angle increases and becomes nearly 90° when waves reach the Buchsbaum resonance. Then waves reflect toward higher L-shell and lower magnetic latitude (e.g., Kim and Johnson, 2015). Because both reflected IIH waves (Kim et al., 2015a) and LHP EMIC waves (Kim and Johnson, 2015) at the Buchsbaum resonance propagate to the different L-shell in dipole field configuration, how 2D/3D heavier ion density structures in the planetary magnetosphere related to propagation characteristics of the IIH and LHP EMIC waves remains as future work.

In summary, we investigate how mode-conversion at the IIH resonance occurs when heavy ion density has along and across inhomogeneity in slab coordinates. The multi-ion simulation results show that the IIH waves have continuous band across the field line, which is consistent with previous numerical studies. These waves also have harmonic structures in frequency and are also localized in the field-aligned heavy ion density well.

Acknowledgements. The work at the Princeton University was supported by NASA grants (NNH09AM53I, NNH09AK63I, NNH11AR07I, NNX14AM27G, and NNH14AY20I), NSF grant ATM0902730, AGS-1203299 and DOE contract DE-AC02-09CH11466. This work was facilitated by the Max Planck/Princeton Center for Plasma Physics. The work at the Kyung Hee University was also supported by the BK21 Plus Program through the National Research Foundation of Korea, funded by the Ministry of Education, Science and Technology.

References

Anderson B. J. et al., The Global Magnetic Field of Mercury from MESSENGER Orbital Observations, *Science 333*, 1859-1862, doi: 10.1126/science.1211001 (2011).

Boardsen S. A. et al., Survey of coherent ~1 Hz waves in Mercury's inner magnetosphere from MESSENGER observations, *J. Geophys. Res. 117*, A00M05, doi:10.1029/2012JA017822. (2012).

Buchsbaum S. J., Ion Resonance in a Multicomponent Plasma, *Phys. Rev. Lett 5*, 495-497 (1960).

Cornwall J. M., Cyclotron instabilities and electromagnetic emission in the ultra low frequency and very low frequency ranges, *J. Geophys. Res. 70*, 61, doi:10.1029/JZ070i001p00061. (1965).

Farmer W. A., Morales G. J., The ion-ion hybrid Alfvén resonator in a fusion environment, *Phys. Plasmas 21*, 062507 (2014), DOI: 10.1063/1.4882662.

Glassmeier K.-H., Klimushkin D., Othmer C., Mager P., ULF waves at Mercury: Earth, the giants, and their little brother compared, *Adv. Space Res. 33*, 1875-1883, doi:10.1016/j.asr.2003.04.047. (2004).

Glassmeier K.-H., Mager P. N., Klimushkin D. Y., Concerning ULF pulsations in Mercury's magnetosphere, *Geophys. Res. Lett. 30*, 1928 (2003).

Horne R. B., Thorne R. M., Wave heating of He+ by electromagnetic ion cyclotron waves in the magnetosphere: Heating near the H+ - He+ bi-ion resonance frequency, *J. Geophys. Res. 102*, 11457 (1997).

Hwang K.-J., Magnetopause Waves Controlling the Dynamics of Earth's Magnetosphere, *J. Astron. Space Sci. 32*, 1 (2015).

Johnson, J., Chang, T., Crew, G. B., A study of mode conversion in an oxygen–hydrogen plasma, *Phys. Plasmas*, 2, 1274-1284 (1995), DOI: http://dx.doi.org/10.1063/1.871339.

Kennel C. F., Petschek H. E., Limit on stably trapped particle fluxes, *J. Geophys. Res. 71*, 1 (1966).

Kim E.-H., Johnson J. R., Full-wave modeling of EMIC waves near the He^+ gyrofrequency, submitted to *Geophys. Res. Lett.* (2015).

Kim E.-H., Lee D.-H., Resonant absorption of ULF waves near the ion cyclotron frequency: A simulation study, *Geophys. Res. Lett. 30*, 2240 (2003).

Kim E.-H., Johnson J. R., Lee D. H., Resonant absorption of ULF waves at Mercury's magnetosphere, *J. Geophys. Res. 113*, A11207. (2008).

Kim E.-H., Johnson J. R., Lee K.-D., ULF wave absorption at Mercury, *Geophys. Res. Lett. 38*, L16111, doi:10.1029/2011GL048621 (2011).

Kim E.-H., Johnson J. R., Lee D.-H., Pyo Y. S., Field-line resonance structure in Mercury's multi-ion magnetosphere, *Earth, Planets, and Space 65*, 447 (2013).

Kim E.-H., Johnson J. R., Valeo E., Phillips C. K., Global modeling of ULF waves at Mercury, *Geophys. Res. Lett. 42*, 5147–5154, doi:10.1002/2015GL064531 (2015a).

Kim E.-H., Boardsen S., Johnson J. R., Slavin J. A., ULF waves at Mercury, *in Low-frequency Waves in Space Plasmas*. American Geophysical Union, Washington, D. C, in press (2015b).

Kim E.-H., Johnson J. R., Kim H., Lee D.-H., Inferring Magnetospheric Heavy Ion Density using EMIC waves, *J. Geophysics. Res.*, 6464, doi:10.1002/2015JA021092. (2015c).

Kim H., Lessard M. R., Engebretson M. J., Luhr H., Ducting characteristics of Pc 1 waves at high latitudes on the ground and in space, *J. Geophys. Res. 115*, A09310, doi:10.1029/2010JA015323. (2010).

Kim H., Lessard M. R., Engebretson M. J., Young M. A., Statistical study of Pc1–2 wave propagation characteristics in the high-latitude ionospheric waveguide, *J. Geophys. Res. 116*, A07227, doi:10.1029/2010JA016355 (2011).

Klimushkin D. Y., Mager P. N., Glassmeier K.-H., Axisymmetric Alfven resonances in a multi-component plasma at finite ion gyrofrequency, *Ann. Geophys. 24*, 1077-1084 (2006).

Klimushkin D. Y., Mager P. N., Marilovtseva O. S., Parallel structure of Pc1 ULF oscillations in multi-ion magnetospheric plasma at finite ion gyrofrequency, *J. Atmos.Solar-Terr. Phys. 72*, 1327, doi:10.1016/j.jastp.2010.09.019 (2010).

Lee D.-H., Lysak R. L., Magnetospheric ULF wave coupling in the dipole model - The impulsive excitation, *J. Geophys. Res. 94*, 17097-17103 (1989).Lee D.-H., Johnson J. R., Kim K., Kim K.-S., Effects of heavy ions on ULF wave resonances near the equatorial region, *J. Geophys. Res. 113*, A11212, doi:10.1029/2008JA 013088. (2008).

Lee D.-H., Lee D.-Y., Shin D.-K., Kim J.-H., Cho J.-H., A Statistical Test of the Relationship Between Chorus Wave Activation and Anisotropy of Electron Phase Space Density, *J. Astron. Space Sci. 31*, 295-301 (2014).

Othmer C., Glassmeier K.-H., Cramm R., Concerning field line resonances in Mercury's magnetosphere, *J. Geophys. Res. 104*, 10369-10378 (1999).

Raines J. M. et al., Structure and dynamics of Mercury’smagnetospheric cusp: MESSENGER measurements of protons and planetary ions, *J. Geophys. Res 119*, 6587–6602, doi:10.1002/2014JA0201 (2014).

Rauch J. L., Roux A., Ray tracing of ULF waves in a multicomponent magnetospheric plasma - Consequences for the generation mechanism of ion cyclotron waves, *J. Geophys. Res. 87*, 8191-8198 (1982).

Russell C. T., Khurana K. K., Arridge C. S., Dougherty M. K., The magnetospheres of Jupiter and Saturn and their lessons for the Earth, *Adv. Space Res. 41*, 1310-1318 (2008).

Song S.-H., Lee D.-H., Pyo Y. S., Wave Model Development in Multi-Ion Plasmas, *J. Astron. Space Sci. 16*, 41-52 (1999).

Taylor W. W. L., Lyons L. R., Simultaneous equatorial observations of 1- to 30-Hz waves and pitch angle distributions of ring current ions, *J. Geophys. Res. 81*, 6177, doi:10.1029/JA081i034p06177. (1976).

Vincena S. T., Farmer W. A., Maggs J. E., Morales G. J., Laboratory realization of an ion-ion hybrid Alfvén wave resonator, *Geophys. Res. Lett. 38*, L11101 (2011), DOI: 10.1029/2011GL047399.

Vincena S. T., Farmer W. A., Maggs J. E., Morales G. J., Investigation of an ion-ion hybrid Alfvén wave resonator, *Phys. Plasmas 20*, 012111 (2013), DOI: 10.1063/1.4775777.

Williams D. J., Lyons L. R., Further aspects of the proton ring current interaction with the plasmapause: Main and recovery phases, *J. Geophys. Res. 79*, 4791, doi:10.1029/JA079i031p04791 (1974a).

Williams D. J., Lyons L. R., The proton ring current and its interaction with the plasmapause: Storm recovery phase, *J. Geophy. Res. 79*, 4195, doi:10.1029/JA079i028p04195 (1974b).

Zurbuchen T. H. et al., MESSENGER observations of the spatial distribution of planetary ions near Mercury, *Science 333*, 1862-1865, doi: 10.1126/science.1211302 (2011).

Figures

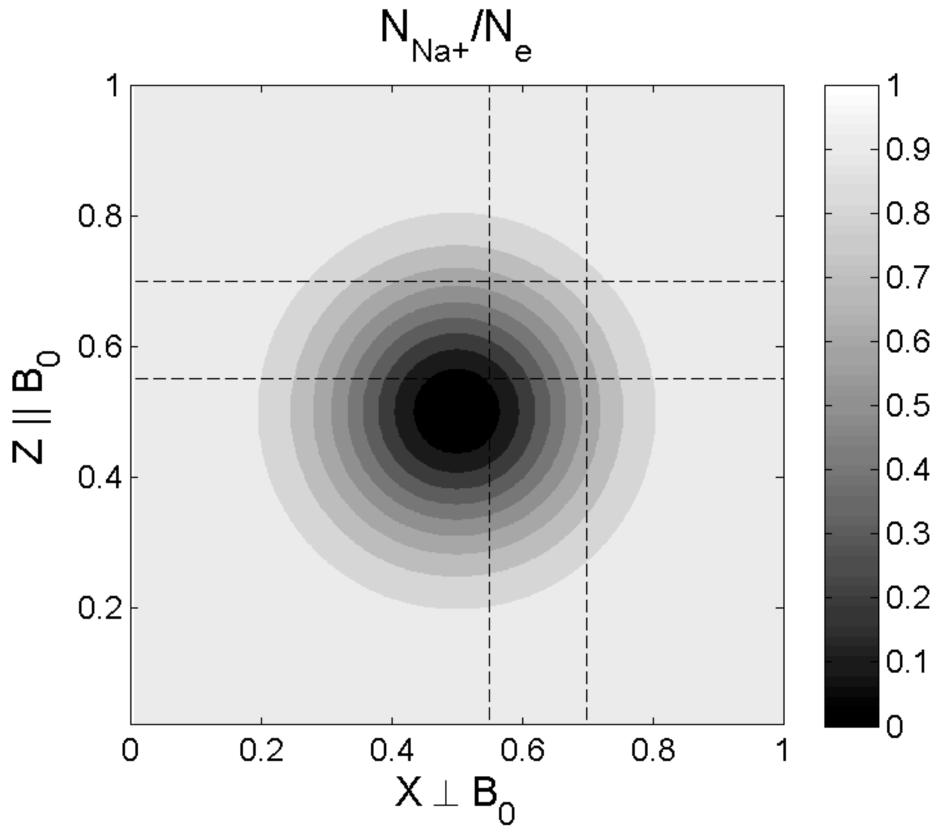

Figure 1. Ratio of Na^+ density to the electron density in *X*-*Z* plane. The sodium concentration has a minimum at the center of the simulation domain. The dashed lines are selected locations of *X* and *Z*; $X_0(Z_0)$ = 0.5 and 0.7 for Figure 3 and 4.

-

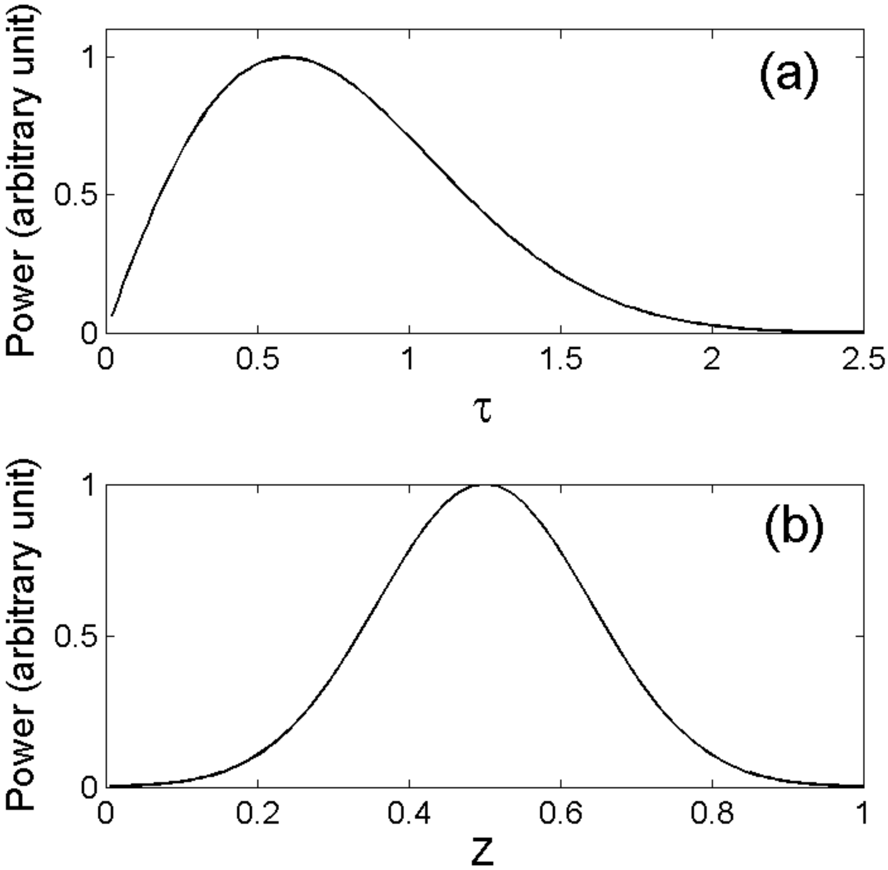

306

Figure 2. Adopted impulsive input (a) in time and (b) in space.

308

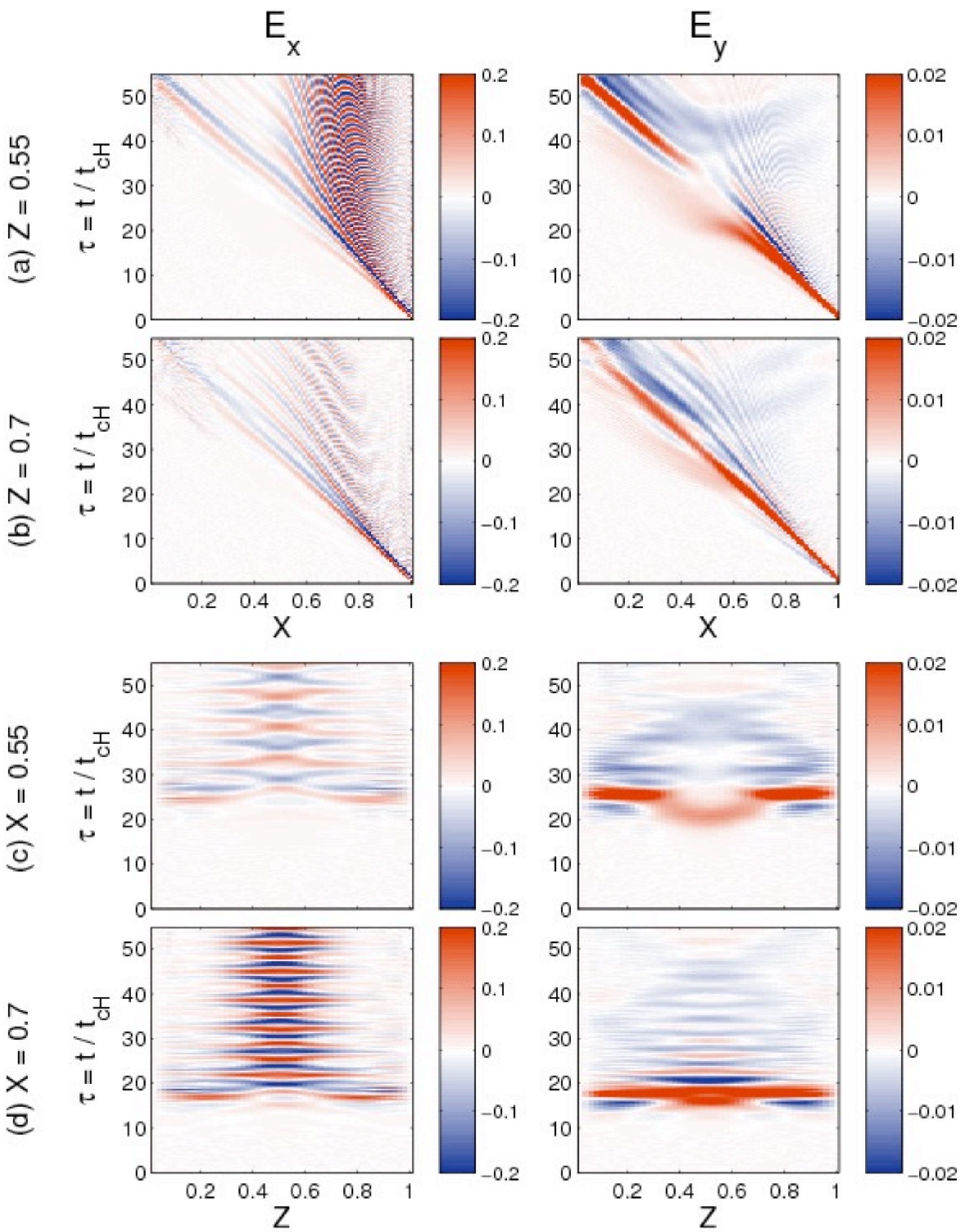

Figure 3. Wave time histories of E_x and E_y along X for (a) Z=0.55 and (b) Z=0.7 and along Z for (c) X=0.55 and (b) X=0.7, respectively.

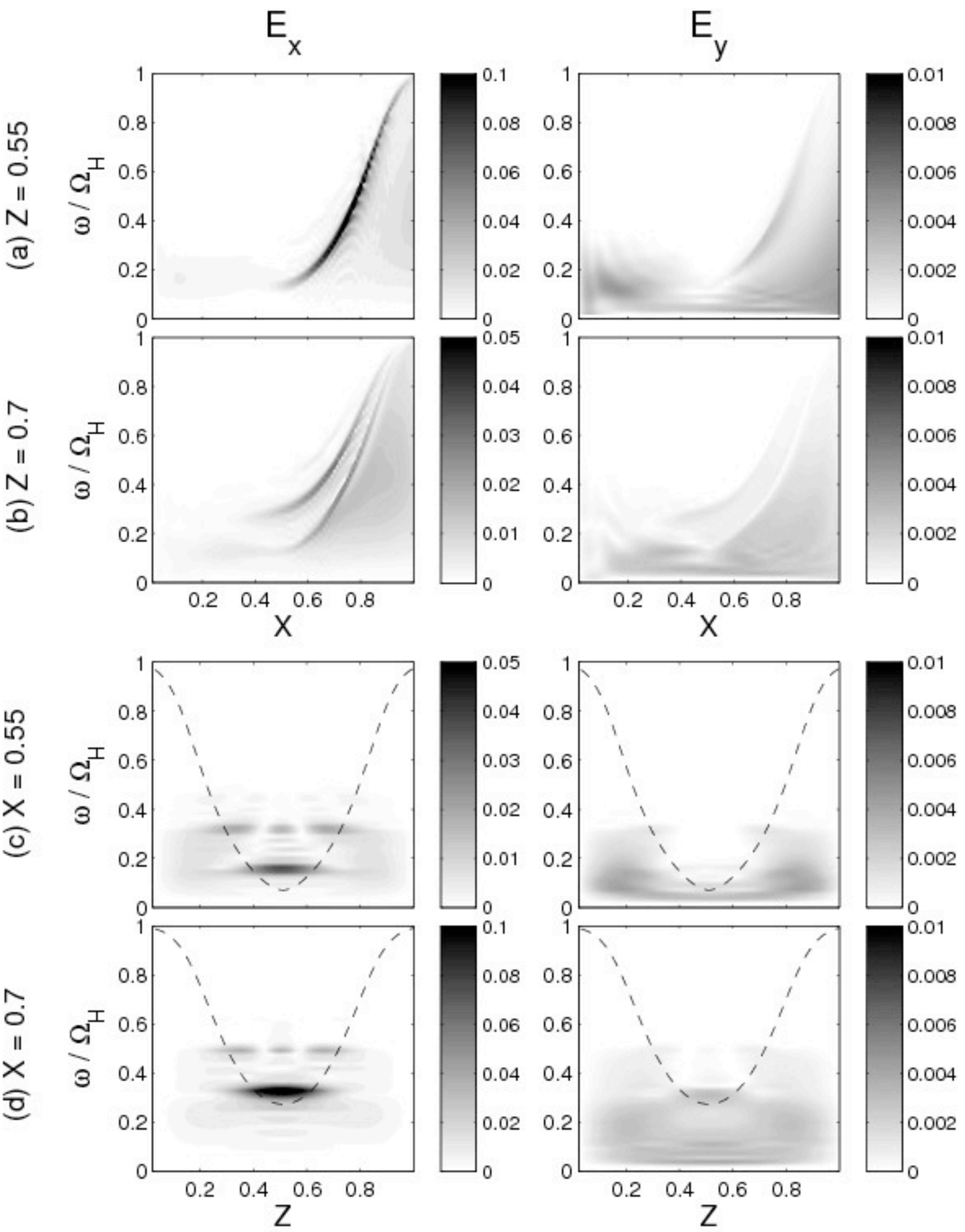

Figure 4. Wave spectra of the E_x and E_y components along X for (a) Z=0.55 and (b) Z=0.7 and along Z for (c) X=0.55 and (b) X=0.7, respectively. Dashed lines represent the calculated Buchsbaum frequencies along Z.

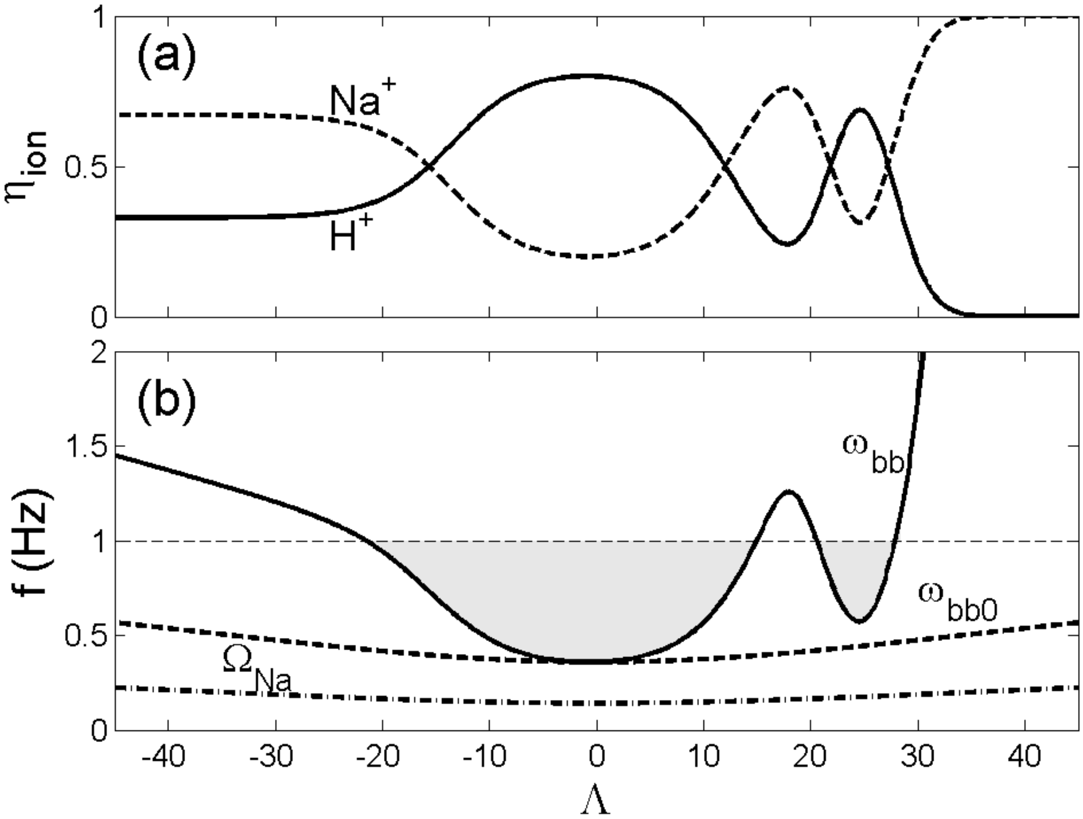

Figure 5. (a) Arbitrary H^+ and Na^+ density ratio along the magnetic field line at L_M=2; (b) Solid line is calculated Buchsbaum frequency along the magnetic field line by adopting heavy ion density ratio from (a), dashed line is the Buchsbaum frequency for η_{Na}=20%, and dashed-dotted line is sodium gyrofrequency. Here, the gray filled area is where IIH wave with 1Hz can propagate, thus IIH waves generated near the magnetic equator can be localized in between -21.7<Λ<15 and 20.5<Λ<27.9.

Princeton Plasma Physics Laboratory
Office of Reports and Publications

Managed by
Princeton University

under contract with the
U.S. Department of Energy
(DE-AC02-09CH11466)

P.O. Box 451, Princeton, NJ 08543
Phone: 609-243-2245
Fax: 609-243-2751

E-mail: publications@pppl.gov

Website: http://www.pppl.gov